ELSEVIER

Journal of Nuclear Materials 290–293 (2001) 579–583

journal of nuclear materials

www.elsevier.nl/locate/jnucmat

Plasma boundary and SOL studies of ECH-plasmas in TJ-II stellarator with diagnosed mobile poloidal limiters

E. de la Cal *, B. Brañas, F.L. Tabarés, D. Tafalla, A.L. Fraguas, M.A. Pedrosa, V. Tribaldos, E. Ascasibar, J. Herranz, I. Pastor, TJ-II Team

Asociación Euratom-Ciemat, Av. Complutense 22, E-28040 Madrid, Spain

Abstract

TJ-II is a medium size (major radius $R = 1.5$ m, average minor plasma radius $a < 0.2$ m, on axis magnetic field $B = 1$ T) helical axis stellarator operating in its first phase with up to 600 kW of ECH power. Two mobile poloidal limiters can control the last closed magnetic surface (LCMS) and diagnose the plasma boundary with a set of Langmuir probes and with CCD-cameras equipped with interference filters. In the described experiments, plasmas with different minor radii interact either with the toroidal limiter or with the mobile poloidal limiters. The electron density and temperature profiles are characterised in the plasma centre, boundary and scape-off layer (SOL) for the different configurations. The global energy for the different configurations is compared and the ratio of the energy confinement time to that obtained by the LHD-scaling-law, seem to be improved when inserting the poloidal limiters. Finally, it is discussed whether the large connection lengths obtained in certain poloidal limiter SOL regions effectively reduce the plasma size, making the definition of the plasma minor radius ambiguous.

Keywords: TJ-II; Limiter; SOL

1. Introduction

In this paper we present the experimental results concerning the influence of the plasma-limiter interaction configuration on the plasma boundary and scrape-off layer (SOL) parameter profiles (electron density n_e and temperature T_e), as well as on the global energy confinement time τ_e. The typical plasma–wall configuration is with the plasma leaning on the toroidal limiter (TL), which consist of thin stainless steel protection plates 360° toroidally around the chamber, where LCMS intersects the vacuum chamber [1]. In this work, we describe the experiments concerning the introduction of two rail-type, stainless steel, mobile poloidal limiters (PL) [2], analysing first the plasma centre, boundary and SOL modification. At first, four plasma configurations with different minor radii and limiter interactions are characterised. Secondly, the SOL connection lengths are analysed theoretically and linked to the particle–flux decays obtained experimentally. Finally, the global plasma energy confinement time is studied for these plasmas and compared with those expected from the scaling-laws. The main result is that the plasmas interacting with the PL have better energy confinement characteristics compared to the plasmas which interact with the TL if we assume that the plasma minor radius is effectively reduced by the limiter insertion.

2. Experimental

The medium size TJ-II stellerator operates in its first phase with up to 600 kW of ECH power ($n_e(0) < 1.7 \times 10^{19}$ m^{-3}) and will operate with 2 MW in about one year. The typical plasma parameters of the experiments described here are: $P^{in} = 300$ kW ECH input power, 200 ms pulse duration, $n_e(0) = 8 \times 10^{18}$ m^{-3} central electron density, $T_e(0) = 800$–1400 eV central electron temperature, $a = 0.12$–0.2 m average minor

* Corresponding author. Tel.: +34-913 466638; fax: +34-913 466 124.

E-mail address: delacal@ciemat.es (E. de la Cal).

0022-3115/01/$ - see front matter
PII: S0022-3115(00)00525-0

plasma radius and helium as working gas. Conditioning of the stainless steel first wall is done every night with a helium glow discharge [3].

Three of the four plasma poloidal cross-sections are plotted in Fig. 1: **A:** interaction with the TL, $a = 0.2$ m, $V = 1$ m^3 plasma volume; **B:** interaction with the mobile PL, $a = 0.16$ m, $V = 0.65$ m^3; **C:** interaction with the mobile PL, $a = 0.12$ m, $V = 0.37$ m^3. The magnetic configuration of plasmas of the type **D** is slightly different (not shown), and is selected so as to have the same magnetic topology as the other cases (same rotational transform, same on axis magnetic field, similar magnetic ripples, etc.), but the LCFS is shifted to the TL so as to reduce the minor radius without introducing the mobile PL: **D:** interaction with the TL, $a = 0.16$ m, $V = 0.65$ m^3. Since the plasma is bean-shaped, the radial minor radius co-ordinater is transformed for each poloidal angle to an effective plasma radius as usually done in these cases.

For plasma characterisation the following diagnostics are principally used: Thomson scattering ($n_e(r)$ and T_e for $r/a < 0.7$), thermal Lithium beam ($n_e(r)$ for $r/a > 0.6$), diamagnetic loop (W_{dia}), reciprocating Langmuir probe, (ion saturation current $I_s(r)$ for $r > a$) and fixed Langmuir probes on the mobile PL ($n_e(a)$ and $T_e(a)$). Other diagnostics used complementary are two CCD-cameras with H_α and HeI interference filters looking on the limiters, microwave-interferometry and ECE-radiometry.

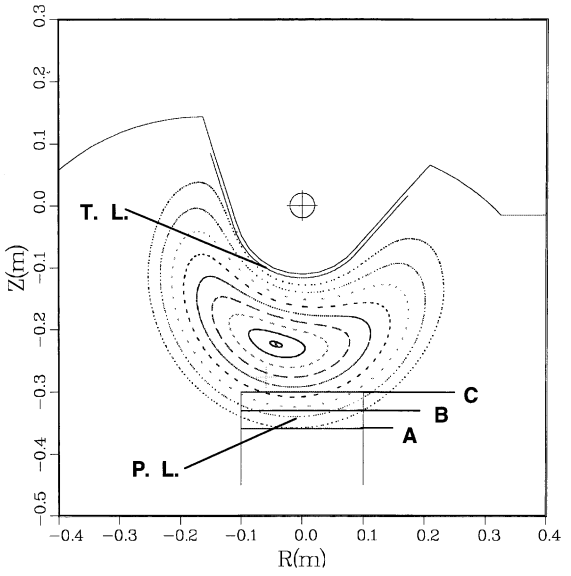

Fig. 1. Poloidal cross-section of three plasma configurations analysed in the experiments (see text), with TL and the mobile PL.

3. Results

Typical plasma parameters obtained for the different configurations with similar conditions (ECH input power $P = 300$ kW, $\langle n_e \rangle = 0.6$–$0.7 \times 10^{19}$ m^{-3}) are listed in Table 1. The electron density and temperature profiles as obtained by Thomson scattering and Lithium beam for configurations **A** and **C** are plotted in Fig. 2. The differential electron-kinetic energy flux tube dW_{e-cin}, whose integration over the plasma radius gives the total kinetic energy W_{e-cin}, is also represented. For the large plasma limited by the TL (case **A**) we can see that the electron density strongly decays at $r = 0.1$ m$(r/a = 0.5)$, as does also dW_{e-cin}. For the smaller plasma limited by the PL (case **C**) this point is shifted to $r = 0.08$ m $(r/a = 0.75$, a being the plasma radius assuming the LCMS at the PL position). In configuration **B** the profiles are similar to **C** (PL) and in **D** similar to **A** (TL).

In Fig. 3(a) the average connection lengths $\langle L_c \rangle$ (average value over 150 different field lines of the same magnetic flux surface) are plotted for the toroidal limiter (TL) and the PL SOL as a function of the minor radius. They are obtained from particle orbit calculations. For field lines with $r > 0.2$ m (TL) $\langle L_c \rangle$ decreases steeply within some millimetres and tends asymptotically to a value of $\langle L_c \rangle = 2$ m. For the PL, SOL this decrease is less steep, since the rail limiters are not poloidally shaped to the plasma LCMS. Within about 10 mm, $\langle L_c \rangle$ is very close to the asymptotic limit of about $\langle L_c \rangle = 23$ m. When analysing the three-dimensional structure of L_c, this naive picture is complicated by the fact that the **PL** introduce strong radial–poloidal–toroidal assymetries in the SOL as demonstrated in Fig. 3(b). In this contour-plot of L_c versus the poloidal and toroidal angles for a given plasma radius two regions can be distinguished: one with $L_c = 13$ m and another one with $L_c = 65$ m, depending on the connec-

Table 1
Typical plasma parameters obtained for the different configurations with 300 kW input power and $\langle n_e \rangle = 0.6$–$0.7 \times 10^{19}$ m^{-3}

Conf.	a (m)	Vol (m^3)	n_e(a) (10^{18} m^3)	$T_e(a)$ (eV)	$T_e(0)$ (keV)	W_{e-cin} (kJ)	W_{dia} (kJ)
A	0.2	1.0	1	8	1	0.27	0.6
B	0.16	0.65	2.5	15	1	0.23	0.5
C	0.12	0.38	4.5	20	0.9	0.15	0.35
D	0.16	0.65	1.3	15	0.8	0.18	0.3

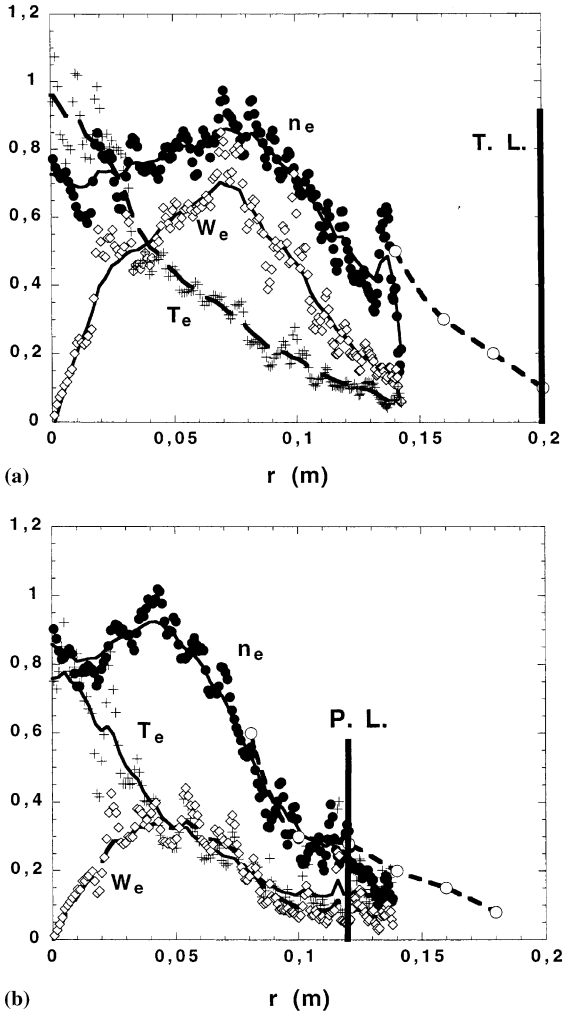

Fig. 2. Electron density $n_e/10^{19}$ m^{-3} ((●) = Thomson scattering, (○) = Li-beam), electron temperature T_e/keV(+ = Thomson scattering) and differential kinetic energy dW_{e-cin}/kJ m^{-1} (◇) profiles for (a) configuration **A** and (b) configuration **C**.

tion of the magnetic flux tubes with the PL. This structure changes for different plasma radii and a three-dimensional topology dominates the SOL. It should be remembered that this L_c-plots are obtained for the vacuum-field case and that the plasma currents and electric fields can modify the real particle orbit trajectories. A flux decay length $\lambda \approx 10$ mm is obtained with the reciprocating Langmuir probe for the TL SOL ($L_c = 2$ m). When inserting the **PL** 4 cm a reduction in the flux by a factor of about 5 is obtained at the TL position and two slopes can be clearly distinguished: in the SOL region dominated by the PL (0.16 m $< r <$ 0.2 m) $\lambda \approx 25$ mm and in the region dominated by the TL ($r > 0.2$ m) $\lambda \approx 10$ mm. The increment by a factor of 2.5 in λ when passing from the TL SOL, with $\langle L_c \rangle = 2$ m, to the PL SOL, with $\langle L_c \rangle = 23$ m, is in good agreement with the simple one-dimensional SOL-model, which predicts a $\lambda \alpha L_c^{0.5}$ dependence [4]. The deduced radial particle diffusion coefficients are typically $D_r = 1.5$ m^2 s^{-1}, similar to that obtained from the Bohm empirical law, $D_B = 0.5$–1.0 m^2 s^{-1}. However, the exponential fit of the flux in the PL SOL is not always linear. With the PL inserted 8 cm and with another magnetic configuration, two different regions appear: for 0.14 m $< r <$ 0.16 m, $\lambda = 25$ mm and for 0.16 m $< r <$ 0.18 m, a very large λ is obtained. This agrees well with the asymmetric SOL picture plotted in Fig. 3(b), in which two regions of different L_c are clearly visible: one with $L_c = 13$ m, which could correspond to $\lambda = 25$ mm and the other to $L_c = 65$ m, corresponding to a much larger λ. More detailed studies, which link the complex stellarator SOL in finite β-plasmas, to non-constant flux-decay lengths were analysed in W7-AS [5]. They are fundamental for the design of divertors.

In Fig. 4 we have represented the experimental energy confinement time τ_{exp}, the ratio of the plasma energy W and the ECH input power P (total absorption is assumed), as a function of the energy confinement time given for each discharge with the LHD-scaling-law τ_{LHD} [6]. The experimental value is obtained for the electron-kinetic contribution W_{e-cin} by integrating the electron density and temperature from the Thomson scattering profiles over the whole plasma volume and also for the global plasma energy content from the diamagnetic loop. A systematic deviation is always present between both methods, since the ion kinetic contribution cannot explain the difference ($W_{i-cin} < 20\%$W with $T_i < 150$ eV). The ratio $H = \tau_{exp}/\tau_{LHD}$ is constant for plasma configurations with TL, but increases when reducing the minor radius with the PL.

4. Discussion and conclusions

TJ-II operates in its first phase at very low densities ($\langle n_e \rangle < 1.2 \times 10^{19}$ m^{-3}) and the low-collisionality plasmas are heated by ECH, which transfers large perpendicular momentum to the electrons. The relative large magnetic ripples, principally in the boundary region, can therefore produce large trapped particle fractions in these conditions and increase the particle and energy losses from the plasmas [7]. This effect could explain the strong decrease for $r/a > 0.5$ in the n_e and T_e profiles shown in Fig. 2 and the somewhat poor confinement found in Fig. 4 (configurations **A** and **D**) compared to scaling-law predictions. These neo-classical effect should be alleviated in the second phase with NBI and much higher densities.

A clear decrease can be seen in the energy content and particle confinement time when the plasma radius is

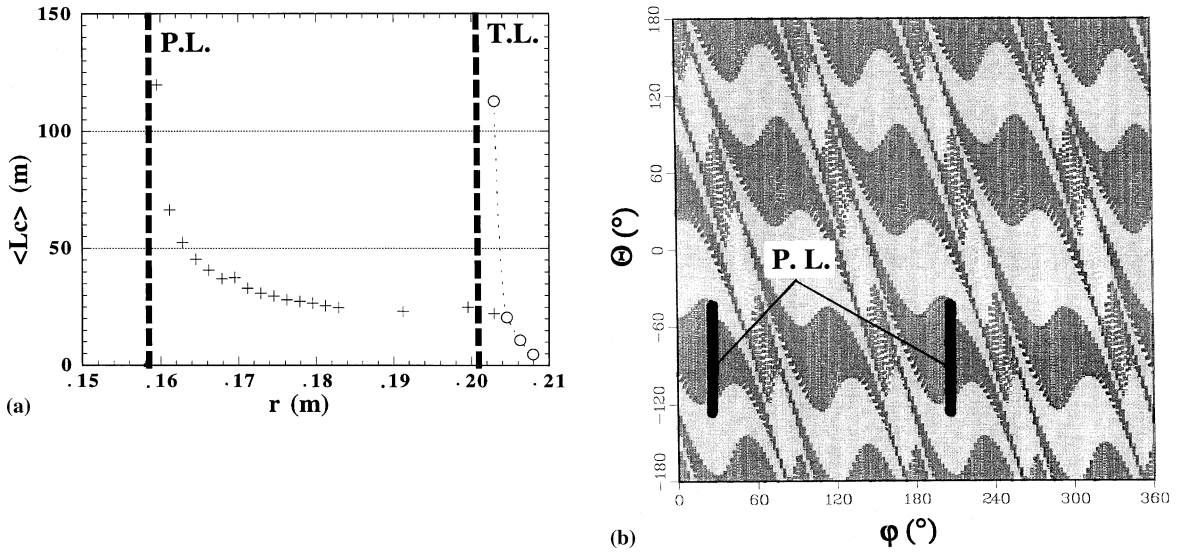

Fig. 3. (a)Theoretical calculation of the average connection lengths $\langle L_c \rangle$ as a function of the effective minor radius for the toroidal (o) and PL SOL (+) and (b) two-dimensional plot of $L_c(\varphi =$ toroidal and $\Theta =$ poloidal co-ordinate): the darker regions correspond to $L_c = 13$ m and the clearer to $L_c = 65$ m.

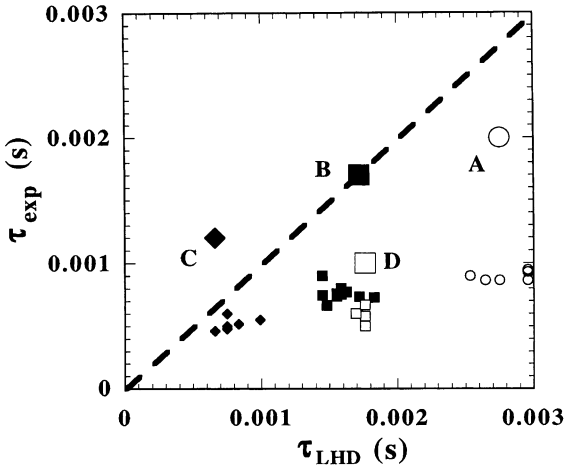

Fig. 4. Experimental energy confinement times τ_{exp} as a function of that obtained by the LHD-scaling-law τ_{exp}. Small symbols correspond to the electron-kinetic estimations and big symbols to that obtained from the diamagnetic loop.

reduced. Most stellarator energy confinement time scaling-laws (e.g., the LHD-scaling) predict a dependence $\tau_E \sim a^2$ [6] and this seems to be true for the TL configurations (plasmas type **A** and **D**). When reducing the plasma radius with the PL the observed reduction in energy confinement time is lower than predicted by the scaling-laws, as was also found in Heliotron-E [8]. If one assumes that the plasma is really reduced in size by the LCFS defined by the PL position, a better confinement is achieved in this condition (τ_{exp}/τ_{LHD} increases by a factor of up to 2 for the plasmas with PL). No significant change in plasma impurity content was found in all configurations, as deduced from bolometer signals. However, the H_α and HeI images show that recycling occurs in a very local way and that fueling should be changed when inserting the PL. The boundary plasma of TL-configurations has a very low electron density (1×10^{18} m^{-3}) and low temperature (10 eV), which should be very transparent to neutrals. It could be possible that in this conditions, the PL SOL can substitute this boundary region, without a so dramatic reduction of the global confinement characteristics with the minor radius, as scaling-laws predict. Another completely different interpretation of the results would be, that the plasma minor radius a is not reduced by the same value as the PL insertion distance. In this case, the ratio $H = \tau_{exp}/\tau_{LHD}$ should be smaller for the PL plasmas than those represented in Fig. 4. However some arguments can be found which would demonstrate that the PL act as the principle sink and source of particles escaping and recycling to the plasma when defining a new LCFS:

- A dramatic change in the H_α images from the cameras is observed, showing a change in the recyling source from the TL to the mobile PL [2].
- The particle fluxes are reduced by a factor of 5 at the TL.
- A global particle balance has been done comparing the particle flux leaving the plasma $F_{out} = N/\tau_p$ ($N =$ total ion density, $\tau_p =$ particle confinement time) and the integrated particle flux reaching the mobile PL measured with the reciprocating Langmuir probe

$F_{\lim} = 0.5 n_e(a)\ c_s\ \lambda\ D$ (c_s = ion acoustic velocity and D = PL extension). A very good agreement is observed between both terms, which let us take the conclusion, that the mobile PL, when inserted 30 mm or more, act as the principle limiters.

These arguments should be taken however with care, since they are deduced from local measurements and we know that the SOL is asymmetric. In fact, particle trajectories in the large L_c-flux tubes produced by the PL SOL could diffuse perpendicularly to the TL, since the parallel PL SOL residence time for the largest connection length $\tau_{ii} \approx L_c/c_s \approx 1 \times 10^{-3}$ s is similar to the perpendicular (radial) residence time in the PL SOL $\tau_r \approx d\lambda/D_r$ (d is the limiter insertion-distance, $\lambda \approx \partial n/\partial r$ the electron density gradient and D_r the radial diffusion coefficient). For these particles the PL is 'absent' and the plasma minor radius is therefore that given by the TL. Further work seems necessary to understand if the PL improve the global confinement characteristics or if this is only a virtual effect due to a bad definition of the effective plasma minor radius.

References

[1] F.L. Tabarés, D. Tafalla, E. de la Cal et al., J. Nucl. Mater. 266–269 (1999) 1273.
[2] E. de la Cal, F.L. Tabarés, D. Tafalla et al., J. Nucl. Mater. 266–269 (1999) 485.
[3] D. Tafalla, F.L. Tabarés, these Proceedings.
[4] A.T. Mense, G.A. Emmert, J.D. Callen, Nucl. Fus. 15 (1975) 703.
[5] F. Sardei, P. Grigull, Y. Feng et al., J. Nucl. Mater. 220–222 (1995) 736.
[6] S. Sudo, Y. Takeiri, H. Zushi et al., Nucl. Fus. 30 (1990) 11.
[7] V. Tribaldos et al., in: Proceedings of the 26th EPS Conference on Controlled Fusion and Plasma Physics, 23J, Maastricht, NL, 1999, p. 349.
[8] S. Sudo, H. Zushi, K. Kondo et al., Nucl. Fus. 31 (1991) 2349.